Concentration Cells

International Edition: DOI: 10.1002/anie.201604790
German Edition: DOI: 10.1002/ange.201604790

Magnetic Cobalt Ferrite Nanocrystals For an Energy Storage Concentration Cell

*Qilin Dai, Ketan Patel, Greg Donatelli, and Shenqiang Ren**

Abstract: *Energy-storage concentration cells are based on the concentration gradient of redox-active reactants; the increased entropy is transformed into electric energy as the concentration gradient reaches equilibrium between two half cells. A recyclable and flow-controlled magnetic electrolyte concentration cell is now presented. The hybrid inorganic–organic nanocrystal-based electrolyte, consisting of molecular redox-active ligands adsorbed on the surface of magnetic nanocrystals, leads to a magnetic-field-driven concentration gradient of redox molecules. The energy storage performance of concentration cells is dictated by magnetic characteristics of cobalt ferrite nanocrystal carriers. The enhanced conductivity and kinetics of redox-active electrolytes could further induce a sharp concentration gradient to improve the energy density and voltage switching of magnetic electrolyte concentration cells.*

Interest in the concentration cell has grown rapidly over the last decade, because of their decoupling nature between energy and power.[1–5] The voltage generated from the concentration cell follows the Nernst equation and has a linear relation with the logarithm of equilibrium concentration ratios. However, the erasing of concentration gradient by diffusion and the electrode corrosion from hazardous byproducts make it challenging to reach a stable energy density, therefore, limiting many applications of concentration cells towards large-scale energy conversion and storage.[6–13] In the meantime, it has been reported that magnetic electrolyte concentration cells (MECCs) utilizes the hybrid interaction between surface redox-active ligands and magnetic nanocrystals as electrolytes, which could readily generate a sharp concentration gradient driven by an external magnetic field.[14] In fact, magnetic nanocrystals are not directly involved in the redox reaction and hence can be recycled as the carrier for redox-active molecules. This prevents the production of any hazardous chemicals, as observed in the conventional concentration cell. Moreover, there is no application of ion-selective membranes which further makes the system cost-effective. High energy density and fast voltage-switching are indispensable for the practical significance of MECCs, which are dictated by the surface coverage density of molecular redox-active ligands, and magnetic characteristics of colloidal nanocrystal carriers.[14] The controllable synthesis of magnetic nanocrystals provides a versatile platform to obtain the optimum particle size and surface features for the adsorption of different redox-active ligands.

Herein, magnetically hard $CoFe_2O_4$ (CFO) nanocrystals are used as the surface carrier for the redox-active citric acid ligands to construct the magnetic electrolyte concentration cell. The oriented attachment (OA) mechanism is utilized to control the growth and magnetic characteristics of CFO nanocrystals, which determine surface attachment of molecular redox-active citric acid ligands and the corresponding concentration gradient under external magnetic field, leading to the tunable voltage output of MECCs. The dimension and crystallinity of CFO nanocrystals largely control their magnetic characteristics, such as saturation magnetization (M_s), remnant magnetization (M_r), and coercivity (H_c, as shown in Figure 1 a–c). The remnant magnetization of hard CFO

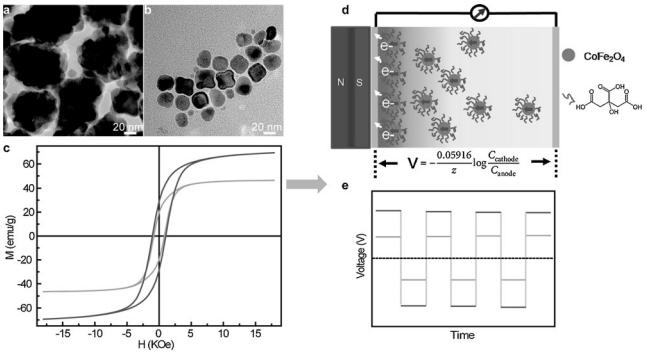

Figure 1. a), b) The CFO nanocrystals with the average diameter of 100 nm and 20 nm, respectively. c) The magnetic hysteresis loops of CFO nanocrystals with the average diameter of 100 nm (light gray curve) and 20 nm (dark gray curve). d) The working principle of MECCs. e) The corresponding voltage output of MECCs with CFO nanocrystal carriers at the average diameter of 100 nm and 20 nm.

nanocrystals maintains the concentration gradient even after removing external magnetic field, and hence energy conversion and storage of MECCs occurs with a very small loss in the total energy. The equilibrium concentration gradient of redox-active citric acid molecules is established by redistribution of magnetic CFO nanocrystals under external magnetic field. The concentration distribution of CFO nanocrystals can be resolved as: $C \approx \exp(A\,M\,H)$, where A is a constant given as μ_0/k_BT (μ_0 is vacuum permeability, k_B is Boltzmann constant, and T is the temperature), H is external magnetic field, and M is magnetic moment of CFO nanocrystals.[14] A constant concentration gradient is established

[*] Dr. Q. Dai, K. Patel, G. Donatelli, Prof. S. Ren
Department of Mechanical Engineering and
Temple Materials Institute, Temple University
Philadelphia, PA 19122 (USA)
E-mail: shenqiang.ren@temple.edu

Supporting information for this article can be found under: http://dx.doi.org/10.1002/anie.201604790.

between two electrodes when the diffusion of citric acid adhered CFO nanocrystals is outweighed by external magnetic force. This also enables the voltage switching (positive to negative) by flipping external magnetic flux (Figure 1 d,e). Based on the Nernst equation, the potential E (V_{output}) of MECCs can be expressed as $E = E_0 - (0.0592/n)*\log Q$, in which n represents the moles of electrons and Q is the concentration ratio between products and reactants.[14]

The CFO nanocrystals play the critical role of carriers for the redox-active citric acid, which makes it essential to synthesize the CFO nanocrystals with controlled size and surface geometry. The typical growth patterns of CFO nanocrystals based on the OA mechanism include three basic steps (Figure 2 a): 1) the formation of primary nanocluster seeds; 2) collision of higher energy surfaces forming the intermediate phases; and 3) formation of monocrystalline structure by coalescence and recrystallization.[15–20] There are two key synthetic parameters based on the OA mechanism, namely reaction temperature and time, governing the structural and morphological evolution of CFO nanocrystals. The effect of the reaction time on the CFO nanocrystal growth is shown in Figure 2 b–d (30 min), Figure 2 e–g (120 min), Figure 2 h–j (240 min), and Figure 2 k–m (360 min) at 593 K. It should be noted that the seeds with average diameter of 20 nm are formed when the reaction takes place for 30 min (Figure 2 b,c). The low crystallinity of the CFO seeds induces the amorphous-like diffraction pattern (Figure 2 d), while {111} surface facets with high surface energy dominate the CFO seed nanocrystals.[21] As the reaction takes place further, the collision among the CFO seeds aggregates along {111} surface facets to minimize the surface energy. The TEM and corresponding selected area electron diffraction (SAED) patterns for the CFO nanocrystals with the average diameter of 100 nm and 200 nm are formed for the reaction time being 120 min and 240 min, respectively (Figure 2 e,h), while the absence of {111} surface facet in the CFO nanocrystals from the XRD spectrum further confirms the collision along high surface energy facets. The corresponding polycrystalline electron diffraction patterns show the aggregation of seeds with different orientations (Figure 2 g–j), which confirm the observation from the TEM images (Figure 2 e,h). The coalescence and recrystallization of CFO nanocrystals take place as the reaction time exceeds to 360 min, forming monocrystalline structures (Figure 2 k–m). The dimension and crystallinity of the CFO nanocrystals largely affect the corresponding magnetic properties, where the CFO nanocrystals formed at 120 min show optimum magnetic performance with M_s of 69 emu g^{-1}, M_r of 28.8 emu g^{-1}, and H_c of 1045 Oe (Figure 2 n).

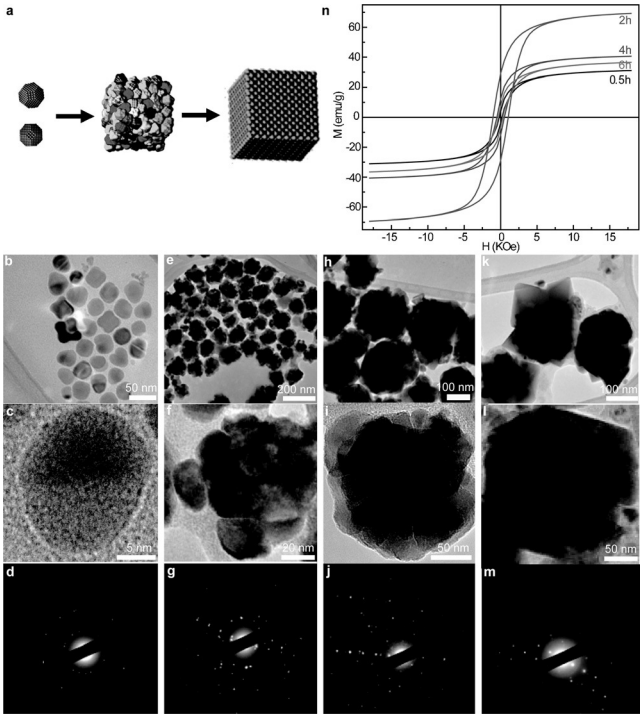

Figure 2. a) The OA growth mechanism of CFO nanocrystals. b)–d), e)–g), h)–j), and k–m) TEM, HRTEM, and SAED images of 20 nm, 100 nm, 200 nm, and 225 nm CFO nanocrystals prepared by the reaction time of 30 min, 120 min, 240 min, and 360 min, respectively. n) Magnetic hysteresis loops of the corresponding CFO nanocrystals.

To further understand the OA-controlled CFO nanocrystal growth, we studied the effects of reaction temperature to control the geometry and dimension of the CFO nanocrystals, which enables the tuning of their magnetic behavior. Figure 3 a–c displays TEM images of the reaction-temperature-dependent size distribution of CFO nanocrystals prepared at 533 K, 573 K, and 593 K, respectively. No crystal formation was observed at the reaction temperature of 533 K. Moreover, the reaction temperature also affects the average dimension of CFO nanocrystals, where a higher reaction temperature induces the smaller CFO nanocrystals (Figure 3 b,c). According to the OA growth mechanism, the short-range and long-range interactions between the CFO nanocrystals are responsible for the collision and coalescence, which is dominated by the reaction temperature. According

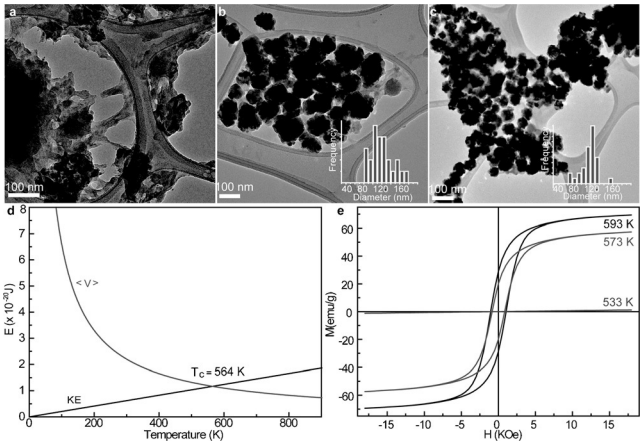

Figure 3. a)–c) TEM images of CFO nanocrystals prepared at different temperatures of 533 K, 573 K, and 593 K. d) The kinetic and dipole–dipole potential energy versus temperature. e) Magnetic hysteresis loops of CFO nanocrystals prepared at different temperatures.

to the results of Leite et al.,[16] there exists an intersection point between the dipole–dipole potentials $\langle V \rangle$ and kinetic energy (Figure 3d), representing a critical temperature (T_c = 564 K). If the reaction temperature exceeds T_c, the kinetic-energy-induced coalescence dominates the OA growth process (Figure 3c), leading to a smaller size of CFO nanocrystals than that of reaction temperature lower than T_c (Figure 3b). Room-temperature magnetic hysteresis loops (Figure 3e) show the optimum magnetic performance (M_s of 69 emu g^{-1}, M_r of 28.8 emu g^{-1}, and H_c of 1045 Oe) of CFO nanocrystals synthesized at 593 K.

With the structural and magnetic control of CFO nanocrystals, their surfaces are further passivated by the redox-active citric acid molecules through the ligand exchange process.[22] The concentration gradient of redox-active molecules is created when an applied magnetic field outweighs the free distribution of the citric acid carrying nanocrystals. The working MECC device under an external magnetic field applied by a pair of Helmholtz coils is shown in Figure 4a. The redox reaction of citric acid takes place at the anode of MECC, and the resulting products include acetonedicarboxylic acid, oxalic acid, and CO_2 (Figure 4b). The O_2 in water is reduced at the cathode to generate OH^-, which is neutralized by H^+ from the oxidation of citrate anion. The overall electrochemical reaction of citric acid is expressed by $HOC(COONH_4)(CH_2COONH_4)_2 + 3O_2 \rightarrow 3HOOC(COONH_4) + H_2O$.[14] A voltage output is observed as the magnetic field is applied to the cell. The performance of the device (voltage output) can be notably controlled by tuning the size of CFO nanocarriers (Figure 4c), which modify surface concentration of citric acid ligands. Furthermore, the sign of voltage output can be switched when the direction of magnetic field is reversed. It is observed that about 60 mV can be obtained for CFO nanocrystals with the average diameter of 10 nm, while the voltage output decreases to 20 mV for 110 nm CFO nanocrystals. The larger surface areas of the smaller nanocrystals improve the device performance as more citric acid can be adsorbed onto the surface of the CFO nanocrystals, which consequently leads to a larger concentration gradient and voltage output. Additionally, the magnetic nanocrystals also enable the response time enhancement of voltage output by varying external magnetic field (Figure 4d). It can be observed that the shortest voltage ramping time, which is determined by the diffusion of CFO nanocrystals under external magnetic field, to reach the maximum voltage output is achieved with an external magnetic field of 5000 Oe. A small magnetic field causes a slow diffusion of CFO nanocrystals, leading to a longer ramping time, and vice versa. As decreasing the applied magnetic field, the maximum voltage output decreases which is attributed to the weak attraction of CFO nanocrystals by a small magnetic field, which, as a result, creates a reduced concentration gradient. It was also observed that the voltage output of MECCs immediately drops by one-third and gets saturated, after the permanent removal of external magnetic field (Figure 4e). This unique feature of MECCs is due to the magnetically hard nature of CFO carriers, which maintains a constant potential difference for a long time between two electrodes without the presence of an external magnetic field. The MECC does not have any voltage output when the citric acid is present in the device in the absence of CFO carriers (Figure 4e), confirming the origin of the voltage output to be possible only when hybrid citric acid–magnetic CFO carriers are present in the electrolyte. Furthermore, to test the recyclability of magnetic CFO carriers, they were re-used after washing and recoating by the citric acid ligands, where both the voltage output and the morphology of CFO nanocrystals remained unchanged (Figure 4f). Therefore, the MECC can be revitalized by just replacing the used citric acid with a fresh batch and there is no need for further synthesizing more CFO nanocrystals for the same cell.

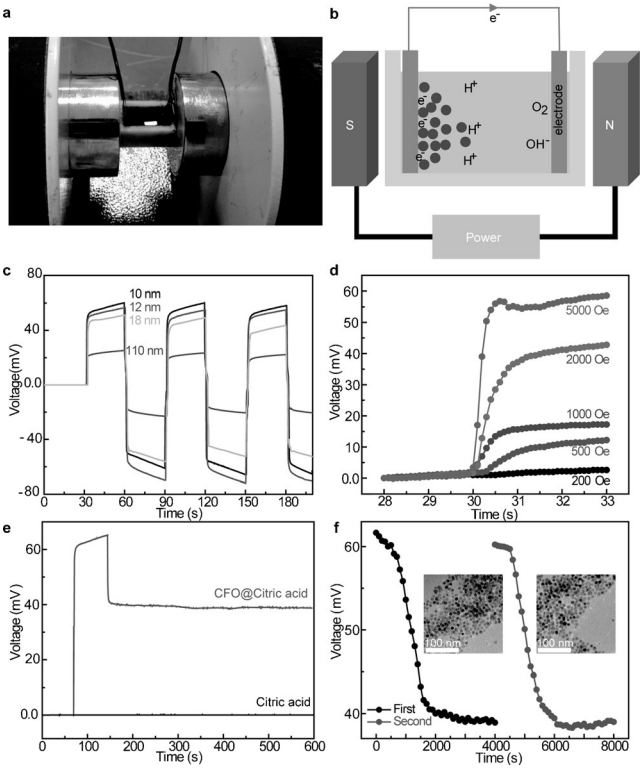

Figure 4. a) Photograph of a working MECC under a magnetic field. b) Diagram of the MECC under magnetic field. c) The voltage output of MECCs based on different sizes of CFO nanocrystals. d) The magnetic field dependent voltage output. e) The voltage output of MECCs based on the citric acid coated CFO and citric acid. f) The stability of MECCs, where each measurement is regenerated by coating the fresh citric acid ligands onto the collected CFO. Insets: corresponding TEM images after the recycling measurement.

The amount of citric acid adsorbed onto CFO nanocrystals, the internal resistance, and the cell dimensions are also the key factors in determining the energy storage performance of MECCs. The voltage output increases with the increase of the molar ratio between magnetic CFO carriers and citric acid ligands (from 1:10 to 1:40; Figure 5a). However, when the CFO carriers reach their surface adsorption limit, any further increase of the citric acid molecules hinders the surface attachment due to the steric effect. As further increasing the concentration of citric acid molecules, this results in a notable decrease in the voltage output of the cell due to the reduced concentration gradient. The addition

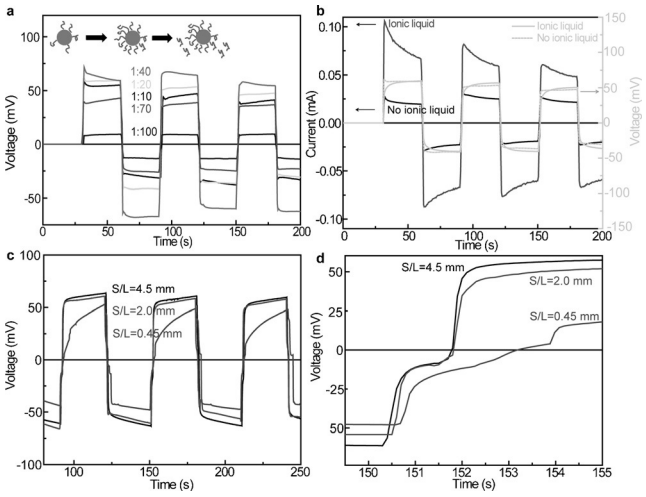

Figure 5. a) Voltage output of MECCs based on different ratios between CFO nanocrystals and citric acid. Inset: mechanism of the excess critic acid, leading to the reduced performance. b) The voltage and current output of MECCs with and without ionic liquid. c) The voltage output of MECCs based on different A/L values. d) The switching time of the voltage output under different A/L.

of an ionic liquid (1-butyl-3-methylimidazolium iodide) into the electrolyte reduces the internal resistance which, consequently, increases the current output of MECCs by 5 times, 0.02 mA→0.1 mA (Figure 5b), while the voltage output is almost the same, indicating that the increased conductivity of the ionic liquid based electrolyte. Furthermore, the voltage output decreases as the cell length increases, which is resulted from a lower concentration gradient from a weak attraction between CFO nanocrystals and external magnetic field. The effect of the cell dimension (constant volume) on the device performance is shown in Figure 5c, in which the optimum cell dimension is determined to be 21 mm × 11 mm × 12 mm (length × width × height). The voltage switching is associated with the redistribution of concentration gradient under different ratios of the surface area of the cell (A) and the cell length (L) while maintaining the external magnetic field at 5000 Oe. The time for voltage switching, which is induced by the switching of the polarity of the nanocrystals, increases either by decreasing the ratio A/L length of the cell or decreasing external magnetic field. Moreover, the kink-type voltage switching behavior is observed as reversing the direction of magnetic flux (Figure 5d), which would drive the re-distribution of citric acid coated magnetic carriers. A weaker magnetic field increases the time for voltage switching as a longer time is needed to re-establish the concentration gradient equilibrium.

Magnetic $CoFe_2O_4$ nanocrystals with controlled dimensions are utilized as the carrier for the surface attachment of redox-active citric acid molecules to construct energy storage magnetic electrolyte concentration cells with fast voltage switching and recyclability. The dimension and crystallinity of CFO nanocrystals are controlled by the OA growth mechanism, in which the tunable magnetic characteristics of CFO nanocrystals dictate the concentration gradient of citric acid and corresponding energy storage performance. Owing to the fact that MECC only requires an external magnetic field to drive the ions in the electrolyte, it can potentially eliminate the use of expensive membranes and pumps to drive the ions, making the conventional flow battery system cost-efficient and feasible for large-scale energy storage.

Experimental Section

The CFO nanocrystals were synthesized by a Schlenk line method. In a typical synthesis, $Co(acac)_2$ (1 mmol) was added in a mixture of oleic acid (5 mL), oleylamine (5 mL), and octadecene (ODE; 5 mL). The resulting solution was degased and purged with Ar gas three times and heated. $Fe(acac)_3$ (2 mmol) in ODE (5 mL) was added in the above solution as the temperature was increased to 433 K. Then degas and purge was applied to the solution. The temperature of the solution was raised to 573 K or 593 K and kept for 2 h, then cooled down to room temperature. After reaction, particles are washed with toluene and acetone three times. Powders were obtained after sample was dried by a nitrogen glovebox.

Room-temperature X-ray powder patterns were obtained by a Bruker D8 advance X-ray powder diffractomer and transmission electron microscope (TEM) images were obtained using a FEOL JEM-1400 microscope. The magnetic hysteresis (M-H) loops were obtained with a Microsense EZ7 vibrating sample magnetometer.

A 3D-printed plastic container was built for the cell. 0.2 mm-thick copper sheets were used as electrodes. An electromagnet was used to supply the magnetic field. A CH electrometer was utilized to collect voltage and current signals. In the measurement, the magnetic field was held for 30 s for each direction. The voltage/current output also varies with the magnetic field.

Acknowledgements

We thank the financial support from the U.S. National Science Foundation (NSF) under the CAREER Award No: NSF-DMR-1551948. Q.D. carried out experiments and wrote the manuscript. K.P. and G.D. helped with the English. S.R. guided the project and edited the paper. All authors discussed the results and commented on the manuscript. The authors declare no competing financial interests.

Keywords: cobalt ferrite · concentration cells · magnetic nanocrystals · oriented attachment

How to cite: *Angew. Chem. Int. Ed.* **2016**, *55*, 10439–10443
Angew. Chem. **2016**, *128*, 10595–10599

[1] P. Alotto, M. Guarnieri, F. Moro, *Renewable Sustainable Energy Rev.* **2014**, *29*, 325–335.
[2] A. J. Bard, L. R. Faulkner, *Electrochemical Methods: Fundamentals and Applications*, Wiley, New York, **1980,** p. 2.
[3] J. O. M. Bockris, A. K. Reddy, *Modern Electrochemistry: An Introduction to an Interdisciplinary Area*, Springer Science & Business Media, Berlin, **1973**, p. 2.
[4] B. A. Grzybowski, K. J. M. Bishop, C. J. Campbell, M. Fialkowski, S. K. Smoukov, *Soft Matter* **2005**, *1*, 114–128.
[5] B. A. Grzybowski, *Chemistry in Motion: Reaction-Diffusion Systems for Micro- and Nanotechnology*, Wiley, Hoboken, **2009**.
[6] B. Jiang, X. Pang, B. Li, Z. Lin, *J. Am. Chem. Soc.* **2015**, *137*, 11760–11767.
[7] W. D. Komhyr, R. A. Barnes, G. B. Brothers, J. A. Lathrop, D. P. Opperman, *J. Geophys. Res. [Atmos.]* **1995**, *100*, 9231–9244.

[8] G. Lagger, H. Jensen, J. Josserand, H. H. Girault, *J. Electroanal. Chem.* **2003**, *545*, 1 – 6.
[9] B. Jiang, C. Han, B. Li, Y. He, Z. Lin, *ACS Nano* **2016**, *10*, 2728 – 2735.
[10] S. Soh, M. Byrska, K. Kandere-Grzybowsk, B. A. Grzybowski, *Angew. Chem. Int. Ed.* **2010**, *49*, 4170 – 4198; *Angew. Chem.* **2010**, *122*, 4264 – 4294.
[11] J. N. Weinstein, F. B. Leitz, *Science* **1976**, *191*, 557 – 559.
[12] J. Xu, D. A. Lavan, *Nat. Nanotechnol.* **2008**, *3*, 666 – 670.
[13] J. Xu, F. J. Sigworth, D. A. LaVan, *Adv. Mater.* **2010**, *22*, 120 – 127.
[14] Y. Yan, J. V. I. Timonen, B. A. Grzybowski, *Nat. Nanotechnol.* **2014**, *9*, 901 – 906.
[15] J. F. Banfield, S. A. Welch, H. Z. Zhang, T. T. Ebert, R. L. Penn, *Science* **2000**, *289*, 751 – 754.
[16] C. J. Dalmaschio, C. Ribeiro, E. R. Leite, *Nanoscale* **2010**, *2*, 2336 – 2345.
[17] M. G. Gong, A. Kirkeminde, S. Q. Ren, *Sci. Rep.* **2013**, *3*, 2092 – 2322.
[18] R. L. Penn, J. F. Banfield, *Science* **1998**, *281*, 969 – 971.
[19] Y. S. Xia, T. D. Nguyen, M. Yang, B. Lee, A. Santos, P. Podsiadlo, Z. Y. Tang, S. C. Glotzer, N. A. Kotov, *Nat. Nanotechnol.* **2011**, *6*, 580 – 587.
[20] Y. S. Xiong, Z. Y. Tang, *Sci. China Chem.* **2012**, *55*, 2272 – 2282.
[21] J. Xie, C. Z. Yan, Y. Zhang, N. Gu, *Chem. Mater.* **2013**, *25*, 3702 – 3709.
[22] S. Q. Ren, L. Y. Chang, S. K. Lim, J. Zhao, M. Smith, N. Zhao, V. Bulovic, M. Bawendi, S. Gradecak, *Nano Lett.* **2011**, *11*, 3998 – 4002.

Received: May 17, 2016
Revised: May 23, 2016
Published online: July 21, 2016

